https://doi.org/10.3311/PPci.43008
Creative Commons Attribution

Periodica Polytechnica Civil Engineering

Generalized Local Curvature Modal Information Entropy (GLCME) for Mitigating Nodal Blindness in Beam Damage Assessment

Zi Yuan[1*], Tianchen Ma[2], Changsheng Xiang[3]

[1] School of Architecture and Civil Engineering, Heilongjiang University of Science and Technology, No. 2468 Puyuan Road, Songbei District, 150022 Harbin, Heilongjiang Province, China
[2] School of Materials Science and Engineering, University of Jinan, No. 336 Nanxinzhuang West Road, Shizhong District, 250022 Jinan, Shandong Province, China
[3] School of Civil Engineering, Lanzhou University of Technology, No. 287 Langongping Road, Qilihe District, 730050 Lanzhou, Gansu Province, China
[*] Corresponding author, e-mail: yuanzi@usth.edu.cn

Received: 08 December 2025, Accepted: 05 October 2026, Published online: 27 October 2026

Abstract

Aiming at the inherent limitation of the curvature mode (CM) index, i.e., its insensitivity to damage near mode shape nodes, this study introduces the concept of generalized local curvature modal information entropy (GLCME) into the CM analysis framework, leveraging the significant potential of information entropy in enhancing damage identification sensitivity. The mathematical formulation of GLCME is rigorously derived, and the corresponding damage index is constructed and optimized by utilizing the characteristics of high-order mode shapes. Numerical models of a simply supported beam and a continuous beam bridge are established to extract and process structural dynamic parameters. Meanwhile, physical tests on a simply supported steel beam are conducted to obtain measured dynamic data for cross-validation. Both CM and GLCME are employed as inputs to a feed-forward neural network (NN) for damage identification, and their performance is systematically compared. The results demonstrate that GLCME enables reliable damage localization and quantification when used as the NN input. Notably, it exhibits significantly higher accuracy and sensitivity than traditional CM, especially in identifying damage near mode shape nodes. The two indices form complementary performance: CM is more suitable for damage far from nodes, while GLCME effectively addresses the challenge of damage identification in nodal regions, providing a more comprehensive technical solution for structural health monitoring of complex bridge structures.

Keywords

curvature modal information entropy, nodal damage identification, damage localization and quantification, beam-type structures, finite element analysis (FEA)

1 Introduction

Structural Health Monitoring (SHM) has become an indispensable paradigm for guaranteeing the safety, serviceability and residual life assessment of bridges, high-rise buildings and wind turbines [1–6]. Among the plethora of vibration-based damage features, curvature mode (CM) shape stands out because its local magnification effect directly links the second-order spatial derivative of displacement to flexural stiffness loss [7–10]. Benefiting from such mechanical clarity, curvature-related indices exhibit remarkable sensitivity in mid-span regions and have been successfully coupled with neural networks (NN), Bayesian inference and compressive sensing to realize simultaneous localization and quantification of damage [11, 12]. Nevertheless, the very same second-order differentiation turns into a critical drawback when damage approaches vibration nodes: near-zero curvatures are overwhelmed by measurement noise, leading to missed alarms and non-unique inverse solutions [13–15]. Moreover, high-order curvature modes, often recruited to enhance spatial resolution, suffer from low signal-to-noise ratios and require densely deployed sensors that are seldom economically viable in long-span bridges [16–20]. Consequently, an urgent methodological gap exists: a universal, single-mode and threshold-free indicator that

Cite this article as: Yuan, Z., Ma, T., Xiang, C. "Generalized Local Curvature Modal Information Entropy (GLCME) for Mitigating Nodal Blindness in Beam Damage Assessment", Periodica Polytechnica Civil Engineering, 2026. https://doi.org/10.3311/PPci.43008

retains the intrinsic merits of curvature while remaining explicitly sensitive to nodal damage is still missing.

Information theory offers a fundamentally distinct perspective from traditional model-driven approaches in structural health monitoring. As a core tool for quantifying the uncertainty of discrete information sources [21, 22], Shannon entropy, together with its derived indicators (e.g., permutation entropy (PE), generalized local entropy (GLE)), has evolved into a model-agnostic metric for "structural disorder" and is widely permeating the field of vibration-based damage identification [23]. The key advantage of these information-theoretic descriptors lies in their ability to amplify damage signatures and suppress environmental noise and measurement errors through fusion techniques (e.g., wavelet entropy [24], relative entropy [25]), while breaking the strong reliance of traditional modal curvature methods on baseline data from intact structures. For instance, the generalized local entropy proposed by Yang et al. [26] identifies local discontinuities caused by cracks using only a single set of measurement data by calculating the Shannon entropy of sliding-window mode-shape sequences; Xiang et al. [27], on the other hand, converts curvature into a probability distribution via a mutual-weight change matrix, whose Shannon entropy forms a baseline-free damage index, and generates "intact" curvature through gapped smoothing technology without relying on pristine reference data. Compared with traditional indicators, entropy-based methods exhibit unique flexibility in integrating heterogeneous monitoring data (e.g., vibration, strain) and adapting to complex service conditions. Their baseline-free characteristic has been validated in practical engineering or simulation scenarios such as the jack-arch segment of the Sydney Harbour Bridge [28] and the Binzhou Yellow River Highway Bridge [29], addressing the application dilemma of traditional methods when baseline data is missing for aging structures.

Despite the progress driven by the aforementioned studies, three critical limitations remain in existing entropy-based methods: First, most entropy variants such as wavelet entropy [24] and Kullback-Leibler divergence [30] rely on full-field or multi-channel signals, which are often difficult to acquire in field bridge monitoring due to sensor installation constraints and associated costs. Second, the threshold setting for entropy changes largely depends on empirical judgment, hindering the autonomous deployment of the technology; third, few studies have directly embedded entropy into the curvature mode shape domain, where the nodal-blind issue (insensitivity to damage near mode shape nodes) is particularly prominent. Therefore, a single-mode, threshold-free, and quantifiable entropy index specifically designed for curvature scenarios is still a research gap, which is the direction this study aims to address. Notably, deep learning has become a mainstream technology in the field of SHM, and its strong capabilities in vibration/image data fusion, nonlinear feature extraction, and real-time baseline-free condition assessment have been fully validated [31–36]. Integrating deep learning with entropy-based indicators is expected to automatically optimize thresholds and feature weights through data-driven approaches, further improving the sensitivity and environmental adaptability of damage identification, and providing a more efficient solution for health monitoring of complex structures, which is also the core research frontier in this field. For future extensions, integrating physics-informed neural networks (PINNs), an approach already explored in some SHM studies [37], could impose structural mechanics constraints on the data-driven fitting process, extending the hybrid framework's interpretability and generalization beyond pure data-driven correction.

This paper proposes, for the first time, the Generalized Local Curvature Modal Information Entropy (GLCME) – a local Shannon entropy operator that acts directly on curvature mode shapes. Framed as a multi-scale damage saliency enhancer, GLCME works analogously to image edge detection and deep learning attention mechanisms [38, 39], serving as a targeted feature magnifier for structural damage. By sliding a three-point window and re-normalizing the central curvature into a probability measure, GLCME converts the classical "near-zero curvature" dilemma into a peak-form entropy anomaly, inherently amplifying node-proximal damage without any user-defined threshold. A lightweight three-layer NN is subsequently trained to map the GLCME vector into residual stiffness, yielding an end-to-end localization and quantification framework that requires only a single mode. Acting as a targeted corrector for node-related insensitivity, this network compensates for modeling uncertainties and measurement noise by learning the nonlinear relationship between GLCME features and actual structural damage states. Numerical studies on a 32 m simply-supported beam and experimental data from a 2.35 m steel beam demonstrate that GLCME reduces the nodal-region relative error effectively, while a continuous-beam model further validates the index under complex bending-moment reversals.

The remainder of the paper is organised as follows: Section 2 derives the GLCME formulation and improved curvature mode for suppressing pseudo-peaks; Section 3 presents simply-supported beam numerical simulations and damage identification via NN; Section 4 describes

simply-supported steel beam experiments, FE modeling, and quantitative validation; Section 5 extends to continuous beam bridges for damage localization and quantification; Section 6 summarizes conclusions and future directions.

2 Generalized local curvature modal information entropy

2.1 Introduction and derivation of indicators

For a discrete set $\{x_i\}$ with probability p_i, Shannon entropy is written as [21],

$$H(X) = -\sum_{i=1}^{n} p_i \ln p_i \,. \tag{1}$$

When the structure is viewed as a collection of independent measuring points, the modal displacement constitutes a discrete spatial process; its local complexity can therefore be quantified by entropy—often termed "mode entropy" in the SHM literature. In this study, the mode shape is treated as a mathematical signal for feature extraction.

To transplant this idea into curvature space, the central-difference curvature at node *i* is defined as

$$\kappa_i = \left(\phi_{i-1} - 2\phi_i + \phi_{i+1}\right)/h^2 \,, \tag{2}$$

where κ_i is the modal displacement and h the uniform mesh size. Within a symmetric window of length n (odd, $n > 3$) centered on i, the total curvature energy is

$$K_i = \sum_{j=i-\frac{n-1}{2}}^{i+\frac{n-1}{2}} \kappa_j \,. \tag{3}$$

The generalized local probability density is then constructed as [26],

$$p_{i,j} = \frac{\kappa_j}{K_i}, \quad j = 1,\ldots,n \,, \tag{4}$$

which satisfies $p_{i,j} > 0$ and normalization condition within the window. Because the weights are derived from curvature rather than from classical probabilities, the resulting index is termed generalized; because only the -point neighborhood is involved, it is termed local.

Substituting the above probability set into the Shannon form yields the GLCME:

$$H_i = -\sum_{j=1}^{n} p_{i,j} \ln p_{i,j} \,. \tag{5}$$

For an intact beam, κ_j is nearly constant, so $p_{i,j} \to 1/n$ and $H_i \to \ln n$ (maximum entropy). Any local stiffness loss distorts the curvature distribution, increases the contrast of and consequently decreases H_i, producing a negative residual that can be used for damage detection. Thus, GLCME inherits the high sensitivity of curvature while circumventing the zero-curvature singularity through the relative weighting approach.

2.2 Selection of probability-calculation window

The window length n in Eq. (3) governs the number of sampling points used to estimate the local probability set. Increasing enlarges the averaging effect, so that slight stiffness loss may be smeared out; simultaneously, more boundary points become unavailable for curvature calculation according to Eq. (5). To quantify this influence, three odd widths $n = 3, 5, 7$, and are compared in Fig. 1. As n grows, the curvature sum inside the window rises, the relative change of caused by a small defect decrease, and the resulting entropy peak becomes lower and wider, leading to reduced positioning accuracy. Thus, a compromise value $n = 3$ is therefore adopted throughout this study, which guarantees at least one genuine curvature extremum inside the window while keeping the computational region minimal.

Substituting $n = 3$ into Eqs. (2)–(4) yields the explicit expression

$$\begin{cases} p_{i-1} = \dfrac{\kappa_{i-1}}{\kappa_{i-1} + \kappa_i + \kappa_{i+1}}, \\ p_i = \dfrac{\kappa_i}{\kappa_{i-1} + \kappa_i + \kappa_{i+1}}, \\ p_{i+1} = \dfrac{\kappa_{i+1}}{\kappa_{i-1} + \kappa_i + \kappa_{i+1}}, \end{cases} \tag{6}$$

and the corresponding GLCME becomes

$$H_i = -\left[p_{i-1} \ln p_{i-1} + p_i \ln p_i + p_{i+1} \ln p_{i+1}\right]. \tag{7}$$

Eq. (7) will be used to compute the first- and second-order GLCME for simply-supported beams. It should be noted that the second-order mode contains a node at mid-span; the near-zero curvature at that location may cause misjudgment, motivating the improvement described in Section 2.3.

2.3 Improvement of the GLCME indicator for higher-order modes

When a curvature mode contains a vibration node, the local curvature κ_i approaches zero. From Eqs. (4) and (5) it follows that

$$\lim_{\kappa_i \to 0} p_i = \frac{\kappa_i}{K_i} \to 0 \,, \tag{8}$$

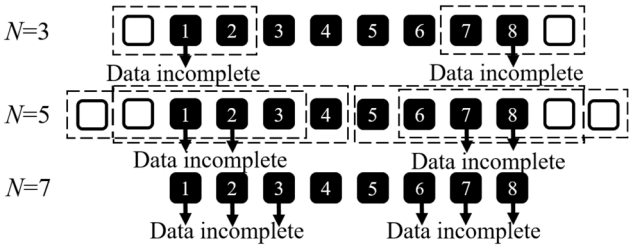


Fig. 1 Local probability window diagram

and consequently,

$$\lim_{\kappa_i \to 0} H_i = -p_i \ln p_i \to 0 \cdot \tag{9}$$

A vanishing entropy peak at the node can therefore mask a genuine damage signature. To eliminate this singularity and enhance the damage feature, we introduce an improved curvature that replaces the near-zero numerator with the maximum curvature magnitude within the entire mode:

$$\kappa_i' = \begin{cases} \kappa_i, & |\kappa_i| \geq \varepsilon, \\ \kappa_{\max}, & |\kappa_i| < \varepsilon, \end{cases} \tag{10}$$

where $\varepsilon = 10^{-6}$ is a numerical stability correction term to avoid singularities in logarithmic operations, and is not a user-defined decision threshold for damage detection. $\kappa_{\max} = \max|\kappa_j|$. The local probability is then re-defined as

$$p_i' = \frac{\kappa_i'}{\sum_{\text{window}} \kappa_j'} \cdot \tag{11}$$

Inserting p_i' into Eq. (5) yields the improved GLCME, H_i'. Equation (10) guarantees a non-zero lower bound for every nodal point, eliminates the spurious entropy valley, and maintains the original vibration trend because $\kappa_{\max}$ is a constant scaling factor within the window. Numerical and experimental results in Sections 4 and 5 confirm that the improved index removes false peaks at mode nodes without shifting the damage location or altering the quantification accuracy.

3 Damage identification of the index in simply-supported beam bridge

3.1 Finite-element model and damage scenarios

To establish a credible and computationally efficient benchmark, a 32 m simply-supported concrete box-girder bridge is selected as the numerical specimen, with its cross-section illustrated in Fig. 2(a). Such proportions represent a typical medium-span highway overpass in Western China [40]. The entire girder is discretized into 32 Euler–Bernoulli beam elements of equal length. C50 concrete is assigned throughout: Young's modulus E = 34.5 GPa, Poisson's ratio ν = 0.20 and unit weight γ = 25 kN/m^3 (Fig. 2(b)).

Damage is introduced as a uniform 20 % reduction of Young's modulus E within a single element. Three locations are selected: mid-span (element 16), quarter-span (element 8), and 1/8-span (element 4), corresponding to the anti-node, 0.5 anti-node, and 0.25 anti-node of the first vertical mode, respectively, as listed in Table 1. These positions allow systematic investigation of the well-known nodal-blind issue without interference from support boundary effects.; each case is analyzed under the same boundary conditions to ensure comparability. A mesh sensitivity study (64 elements vs 32 elements) reveals frequency changes <0.1 %, confirming that the adopted discretization is already convergent. Thus, the 32-element model represents an optimal balance between accuracy and computational cost for the present study.

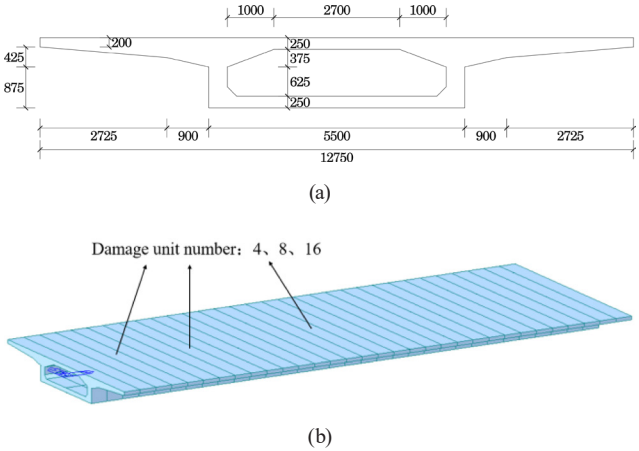
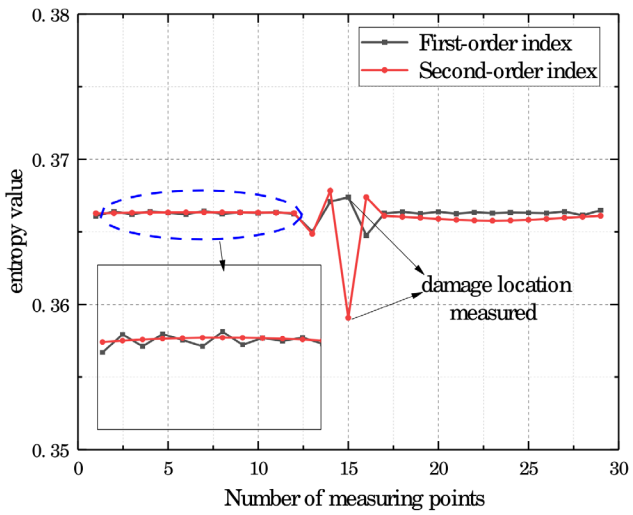


Fig. 2 Geometric structure and analysis model of simply-supported beam bridge: (a) Cross section of the simply-supported bridge; (b) FEA model of simply-supported beam bridge

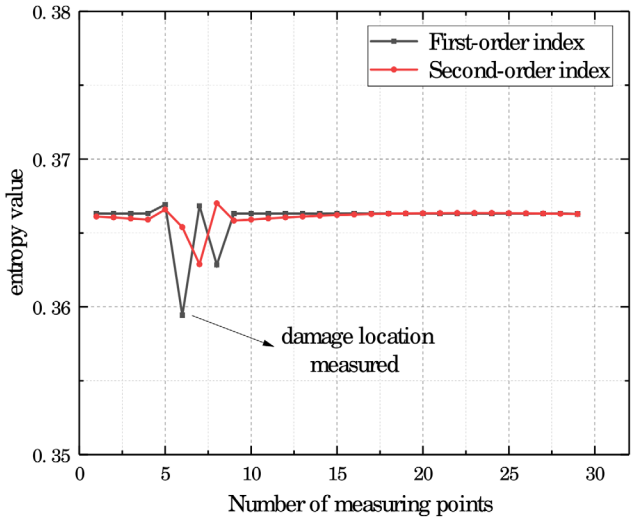
Table 1 Damage condition of finite element model

Scenario	Damage element	Damage location	Severity
2–1	16	1/2-span	
2–2	8	1/4-span	20 % E
2–3	4	1/8-span	

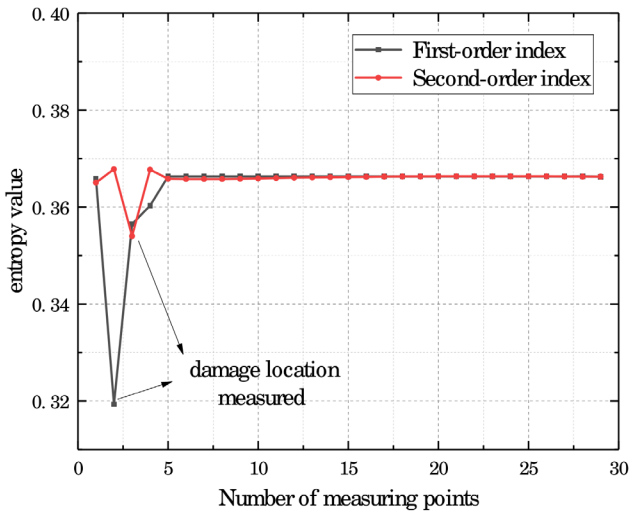
Owing to locked vertical degrees of freedom (DOFs) at both supports, the model retains only 29 equally spaced nodes. First and second-order vertical modes are incorporated into Eq. (6) to generate Fig. 3. This figure demonstrates a clear modal dependence. Damage coinciding with the curvature extremum of a given mode triggers an immediate sharp peak in the corresponding order of GLCME while damage outside the extremum zone only results in a shoulder or slight offset. Mid-span damage is governed by the second order whereas quarter and 1/8-span damage are dominated by the first order, with a systematic offset of approximately one element that increases as damage moves away from the curvature peak. This drift arises from the combined effects of discrete mesh spacing and modal shape and does not represent a methodological flaw. Notably, the second-order curve exhibits global smoothness with gentle peak-to-valley transitions, indicating stronger stability under noisy conditions. This feature will be further verified through mesh refinement and experimental tests in subsequent studies. Overall, the GLCME confines single damage to the adjacent element range and provides an intrinsic relative-contrast alarm, thus offering a reliable baseline for future improvements.



(a)



(b)



(c)

Fig. 3 Damage recognition results of first-two orders index: (a) Damage scenario 2–1; (b) Damage scenario 2–2; (c) Damage scenario 2–3

3.2 Damage quantitative method and verification based on neural network

For practical blind inspection scenarios with unknown damage locations, a three-step workflow is adopted: (1) locate the suspected damage region via GLCME amplitude peaks; (2) select GLCME and curvature values of the three nearest nodes to the peak; (3) feed the 3-D vector into the neural network for stiffness quantification.

A three-layer feed-forward network is trained with Levenberg-Marquardt back-propagation to map local damage features into residual stiffness. For each detected damage location, the original GLCME and curvature values of the three nearest nodes are concatenated into a 3-D input vector. Training samples are generated by reducing Young's modulus to 10 %, 15 %, 25 % and 30 % at the same three span positions, yielding 36 combinations (3 locations × 4 severities × 3 replicates). The target output is the non-dimensional residual stiffness Edamaged/Eintact of the damaged element. Training is stopped when the mean-square error falls below 10^{-7} or the epoch count reaches 50, whichever occurs first. The damage identification results are shown in Table 2.

Table 2 summarizes the network predictions under the damage scenario 2-1–2-3. A consistent modal-dependence is observed: when damage approaches the anti-node of a given mode, the same-order GLCME-NN pair yields sub-5 % relative error; when the damage is close to the node, the complementary-order pair takes over and maintains the same accuracy. Specifically, at quarter-span (element 8) the first-order GLCME-NN gives 4.88 % error, whereas the second-order gives 1.50 %; at 1/8-span (element 4) the roles reverse (8.25 % vs 1.88 %). Thus, first- and second-order GLCME provide quantitative accuracy that complements each other, retaining <5 % error when damage lies within 0.1 L of the corresponding modal anti-node. The network weights are stored once and reused for all test cases, demonstrating that a single 3-5-1 architecture trained on pure FE data is sufficient for sub-element stiffness estimation without retraining or transfer learning.

4 Test validation on simply-supported beam bridge

To establish a reliable link between numerical benchmarks and physical experiments, a precision-manufactured simply-supported steel beam was tested. Full details of the specimen and experimental setup are provided in Section 4.1.

4.1 From numerical benchmark to laboratory specimen

A simply-supported steel beam (total length 2350 mm, cross-section 100 mm × 8 mm, calculated span 1750 mm) is

Table 2 Damage quantitative damage recognition results

Order	Scenario	Number of element	CM	GLCME	Ideal output	absolute error of CM	absolute error of GLCME	relative error of CM	relative error of GLCME
First-order index	2–1	No.16	0.815	0.777	0.8	0.015	0.023	1.88%	2.88%
	2–2	No.8	0.761	0.833	0.8	0.039	0.033	4.88%	4.13%
	2–3	No.4	0.869	0.811	0.8	0.069	0.011	8.25%	1.38%
Second-order index	2–1	No.16	0.864	0.791	0.8	0.064	0.088	8.00%	1.10%
	2–2	No.8	0.782	0.788	0.8	0.018	0.012	2.25%	1.50%
	2–3	No.4	0.785	0.873	0.8	0.015	0.073	1.88%	9.12%

precision-milled and pre-drilled to ensure repeatable bolted boundary conditions, as shown in Fig. 4. Tensile coupons yield 432 MPa yield strength and 198.9 GPa Young's modulus; the acquisition chain and accelerometer layout are detailed in Fig. 4.

4.1.1 Damage scenario definition

A single steel beam (Beam-1) was utilized to implement different damage scenarios through progressive machining, eliminating the influence of specimen-to-specimen variability. The specific damage configurations are summarized in Table 3:

- Undamaged state: The as-manufactured Beam-1 without any artificial defects, serving as the baseline for comparison.
- Damage scenario 3-1: After completing the undamaged state tests, the beam was returned to the manufacturing facility for machining a 25 mm-deep × 10 mm-wide notch at 300 mm from the support center (with the support center as the origin).

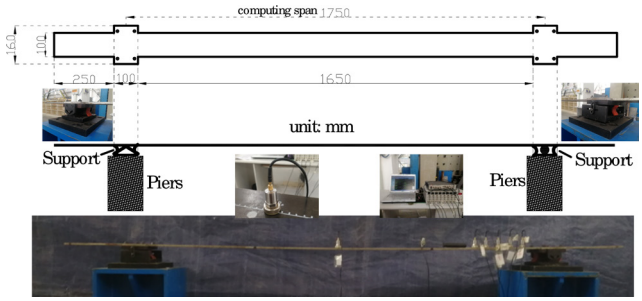


Fig. 4 Geometry of the steel beam and layout of the data acquisition system (Unit: mm)

Table 3 damage cases of the steel beam

Specimen	Damage scenario	Damage configuration
Beam-1	scenario 3-1	25 mm-deep×10 mm-wide notch at 300 mm from the support center
	scenario 3-2	25 mm-deep×10 mm-wide notch at 300 mm and 875 mm from the support center

- Damage scenario 3-2: Subsequent to the tests under scenario 3-1, an additional 25 mm-deep × 10 mm-wide notch was machined at the position of 875 mm from the support center, resulting in a multi-damage configuration.

4.1.2 Measurement point arrangement and testing methodology

Considering the size of the sensor base and the actual dimensions of the steel beam, a spacing of 50 mm between adjacent measurement points was determined. For data analysis, the mode shape components at the centers of the two supports were assumed to be consistent with the theoretical value of 0. A total of 34 measurement points were arranged along the beam. Specifically, Point 1 was located 50 mm from the center of the fixed hinge support, and Point 34 was 50 mm from the center of the rolling support, with the remaining points uniformly distributed between them. The detailed layout of the measurement points is presented in Fig. 5.

The hammer impact test was adopted for modal data acquisition. Given the availability of 6 high-frequency accelerometers in the laboratory, a roving reference test strategy was designed. In each test group, one sensor was fixed as a reference point, while the remaining five sensors were placed on five consecutive measurement points. A total of 7 test groups were required to cover all 34 measurement points. The excitation was applied near the reference point using an instrumented hammer to trigger data sampling. For each test group, three sets of data were collected, and the average value was used for subsequent analysis to minimize random errors.

Preliminary calculations revealed that the peak of the first-order mode shape occurs at the mid-span, which coincides with the node of the second-order mode shape. In contrast, the second-order mode shape reaches its peak at the 3/4 span position and exhibits an opposite direction to the first-order mode shape. Based on these characteristics, the reference point was strategically set at Point 18 when acquiring the first-order mode shape, and at Point 26 (near

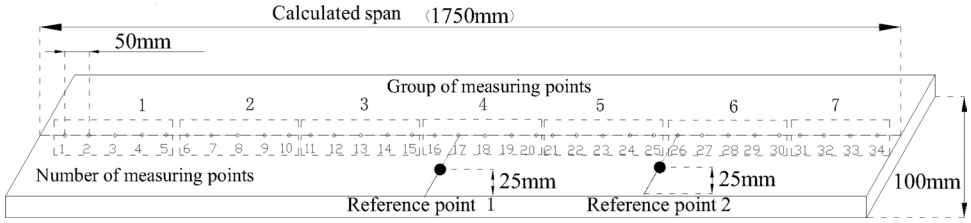


Fig. 5 Measuring point layout for modal testing

the 3/4 span position, i.e., 1312.5 mm from the support center) when acquiring the second-order mode shape.

For the first two orders of modes, after collecting the acceleration responses, the random subspace identification (SSI) method was employed to analyze the time-domain waveform data. Mode shape normalization and mass normalization were performed with reference to the pre-determined reference points to extract the vertical mode shape components of the first two orders. Finally, the data was preprocessed through filtering to obtain the damage identification results. The on-site testing and data acquisition process are shown in Fig. 6.

4.2 Finite element modeling of the test structure

To facilitate effective comparison and validation of the experimental data, two finite element (FE) models were established using MIDAS/Civil [41] and ANSYS [42] software, respectively, strictly following the actual dimensions and material properties of the test specimen.

For the MIDAS/Civil model, the beam was discretized into 235 beam elements with a length of 10 mm each, covering the full-length of 2350 mm. For the ANSYS model, solid185 elements were adopted, and the model was meshed using hexahedral elements with a mesh size of 4 mm through the sweeping method. Material properties derived from the tensile coupon tests were assigned to both models: elastic modulus of 198.9 GPa, Poisson's ratio of 0.3, and the corresponding density is 7.698×10^{-5} N/mm^3. The FE models for Damage Scenario 3-1 are presented in Fig. 7.

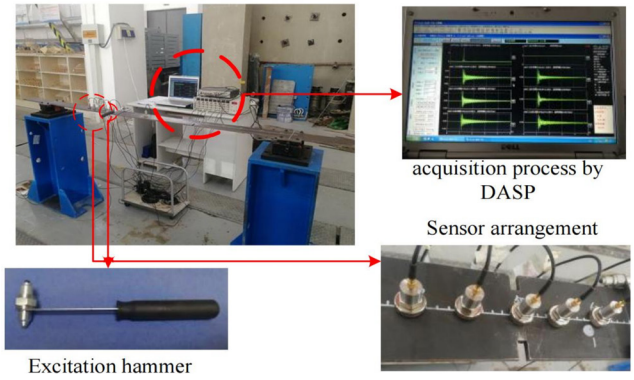


Fig. 6 Modal test site

Modal analyses were performed on both FE models to obtain the first two orders of mode shapes. The mode shapes from ANSYS, MIDAS/Civil, and the experimental measurements were all normalized to ensure consistency. These normalized mode shapes were then substituted into Eqs. (2)–(7) to calculate the first two orders of curvature mode shapes and the GLCME. The damage identification results are presented in Fig. 8.

4.3 Quantitative damage identification based on neural network

A three-layer NN was employed for quantitative damage identification, consistent with the previous configuration. A comprehensive training dataset was constructed, encompassing 18 damage scenarios with varying hole

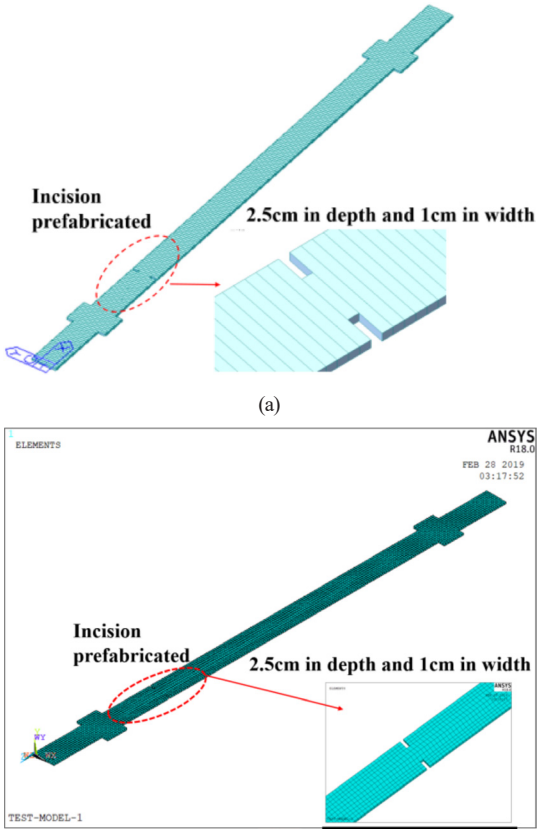


Fig. 7 Finite element models under different damage scenarios: (a) MIDAS/Civil model for scenario 3-1; (b) ANSYS model for scenario 3-1

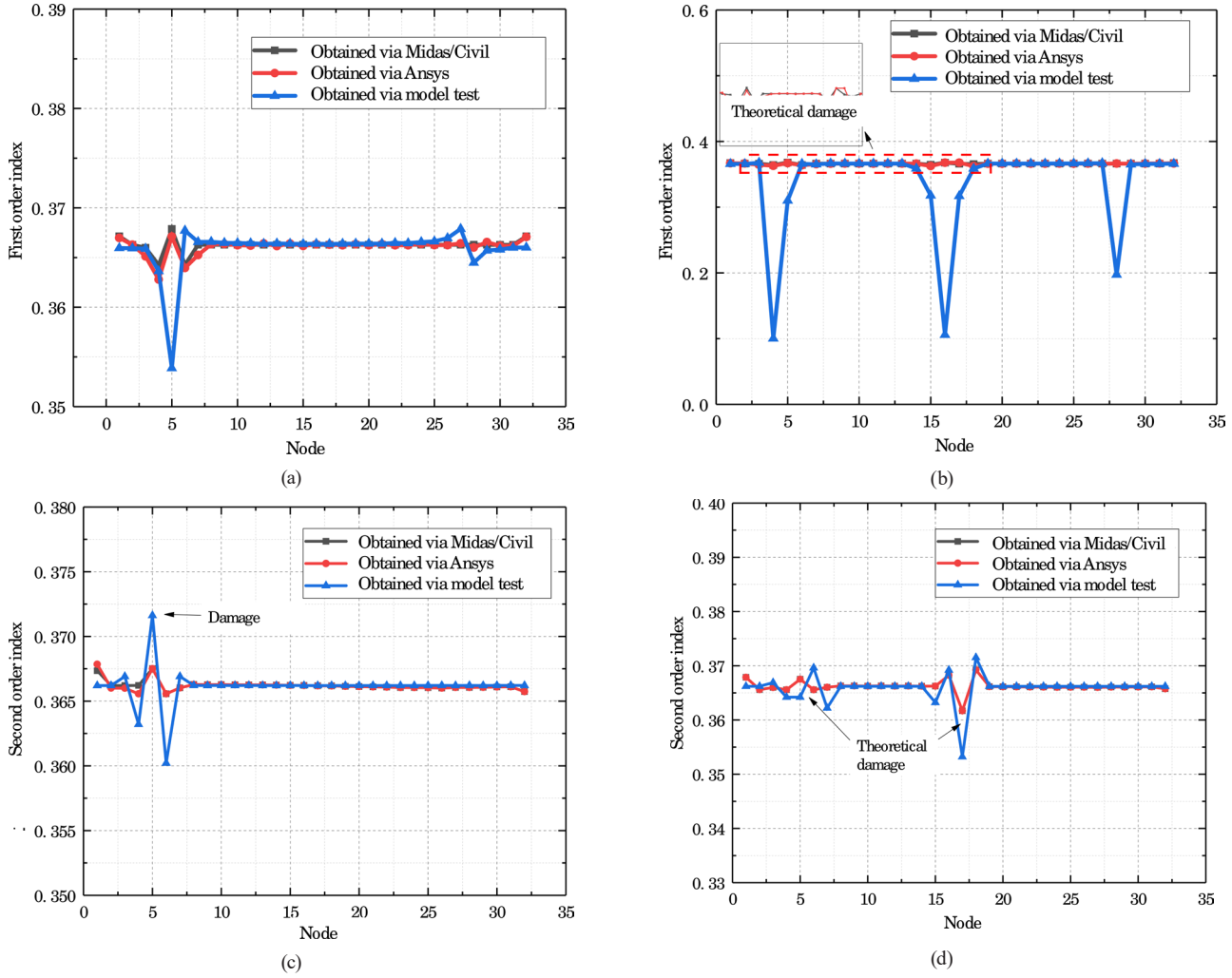


Fig. 8 Measured and theoretical damage locations identified by the proposed index: (a) Identification result of the first-order index for scenario 3-1; (b) Identification result of the first-order index for scenario 3-2; (c) Identification result of the second-order index for scenario 3-1; (d) Identification result of the second-order index for scenario 3-2

depths at two predefined locations (including simultaneous double damage).

The parameters of the NNs were set identically to those in the previous section, with the residual stiffness of the damaged element as the output variable. The optimal number of hidden layer nodes was determined to be 11 through parametric analysis, resulting in a network structure of 3-11-1 (input layer-hidden layer-output layer). The quantitative damage identification results are summarized in Table 4.

4.4 Discussion of experimental results

A comparative analysis of the first two orders of indicators reveals that the quantitative damage identification accuracy of the first and second-order curvature mode indicators at their respective mode shape nodes is lower than that of the proposed generalized local curvature mode information entropy. Specifically:

- Near the first-order mode shape node (300 mm from the support center), the quantitative relative error of the curvature mode indicator reaches 72.94%, while the error of the proposed index is significantly reduced to 20.0%.
- Near the second-order mode shape node (875 mm from the support center), the relative error of the curvature mode indicator is 34.8%, which is also higher than the 20.0% error of the proposed index.

Furthermore, for both damage scenarios, the identification accuracy of all indicators at the mode shape nodes is consistently lower than that at positions far from the mode shape nodes. This observation validates the conclusion proposed in the previous section, confirming the superiority of the generalized local curvature mode information entropy in avoiding the "node effect" and improving damage identification accuracy.

Table 4 Quantitative identification result of damage of simply supported steel beam

Index order	Damage scenario	Damaged element node no.	CM	GLCME	Ideal output	Absolute error of CM	Absolute error of GLCME	Relative error of CM	Relative error of GLCME
First-order index	3-1	No.6 (30cm)	0.422	0.436	0.5	7.77%	6.38%	15.5%	12.8%
		No.18 (87.5cm)	1	1	1	0%	0%	0%	0%
	3-2	No.6 (30cm)	0.865	0.400	0.5	36.5%	10.0%	72.9%	20.0%
		No.18 (87.5cm)	1.000	0.477	0.5	50.0%	2.31%	100%	4.62%
Second-order index	3-1	No.6 (30cm)	0.46	0.436	0.5	4.00%	6.38%	8.00%	12.8%
		No.18 (87.5cm)	0.984	0.999	1	1.60%	0%	1.60%	0%
	3-2	No.6 (30cm)	0.352	0.421	0.5	14.8%	7.90%	29.6%	15.8%
		No.18 (87.5cm)	0.326	0.400	0.5	17.4%	10.0%	34.8%	20.0%

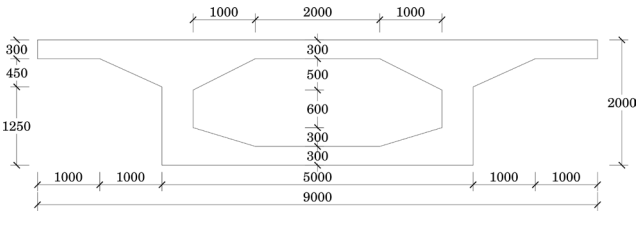
5 Damage identification of the index in continuous beam bridge

Continuous beam bridges exhibit superior spanning capacity due to the unloading effect of negative moments at supports, making them widely applicable in modern transportation infrastructure to meet the evolving demands of bridge engineering. To further verify the robustness and applicability of the proposed index, this chapter extends the research scope from simply supported beams to continuous beam bridges, systematically investigating the performance of the generalized local curvature mode information entropy in damage identification for such structures.

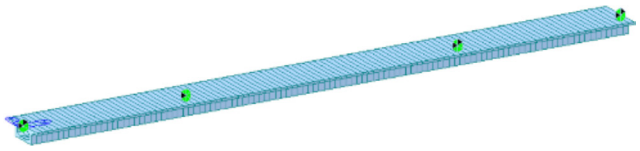
5.1 Model establishment and damage scenario definition

A key distinction in mode shapes between continuous beams and simply supported beams lies in the presence of support constraints, which cause each mode shape to intersect with the structural baseline. A three-span continuous beam bridge model was established using MIDAS/Civil, featuring a box-section girder as illustrated in Fig. 9(a). The overall layout and constraint conditions of the bridge model are presented in Fig. 9(b). The bridge has a span arrangement of 30 m + 50 m + 30 m, with a total of 111 nodes and 110 elements (each element is 1 m in length). The main girder is constructed of C50 concrete, with material properties as follows: elastic modulus of 3.45×104 MPa, Poisson's ratio of 0.2, and bulk density of 25 kN/m^3. The adoption of a three-span configuration with unequal spans aligns with practical engineering applications. Notably, the negative bending moment at the mid-span results in zero points of the curvature mode near the supports, as shown in Fig. 10. The specific constraint conditions for the continuous beam are detailed in Table 5.

Figs. 11 and 12 present the damage identification results of the GLCME for the continuous beam before and after improvement, respectively. It is evident that the spurious peaks in the unimproved index are eliminated after



(a)



(b)

Fig. 9 Geometric structure and analysis model of continuous beam bridge: (a) Cross section of the continuous beam bridge; (b) FEA model of continuous beam bridge

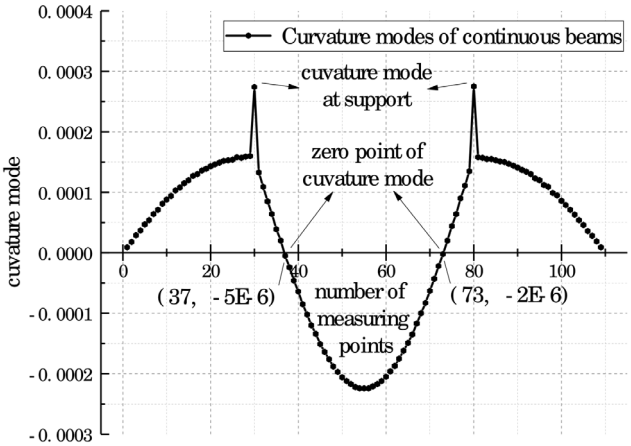


Fig. 10 First-order curvature model of continuous beam

Table 5 Constraints for continuous beams

Node	D_x	D_y	D_z	R_x	R_y	R_z
1	×	√	√	√	×	√
31	√	√	√	√	×	√
81	×	√	√	√	×	√
111	×	√	√	√	×	√

Note: "√" indicates a constrained degree of freedom; "×" indicates an unconstrained degree of freedom.

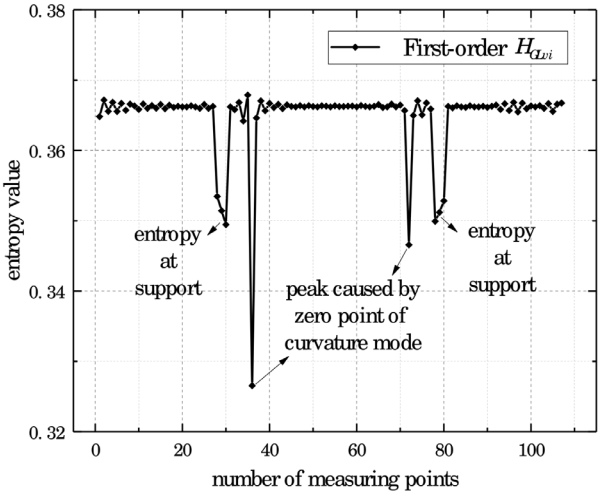


Fig. 11 Result with index unimproved

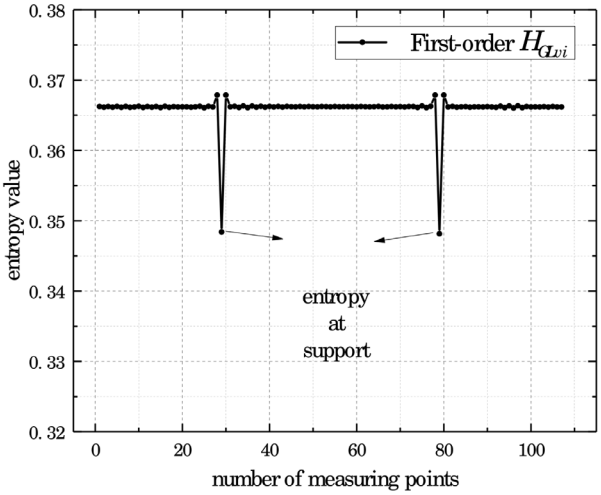


Fig. 12 Result with index improved

optimization. For the peaks at the supports, the corresponding entropy values remain unchanged while the peak width is narrowed, which mitigates the interference of support-related peaks on damage location identification. Additionally, the improved index exhibits a smoother distribution, facilitating more accurate damage localization and quantification.

Damage scenarios were defined by simulating stiffness reduction, with the second span (mid-span) selected as the primary research object. The specific damage configurations are summarized in Table 6.

Table 6 Damage conditions of continuous beams bridges

Damage conditions	Node	Damage degree	Damage location
5-1	55	20%	Mid-span
5-2	38	20%	Zero point of the curvature mode
5-3	35	20%	Near the support (mode node)

5.2 Damage localization results of the proposed index

Modal analysis was performed on the continuous beam model under various damage scenarios. The vertical mode shapes were extracted and substituted into Eqs. (3)–(10) to calculate the first-order generalized local curvature mode information entropy, with the damage localization results plotted in Fig. 13.

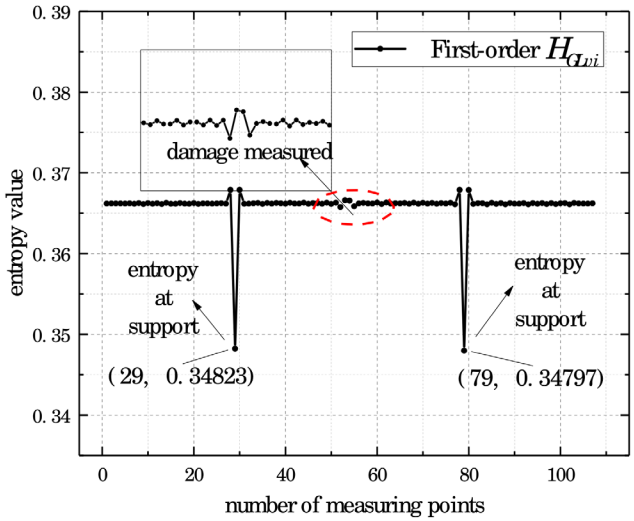
Fig. 13 reveals key patterns of damage identification in continuous beam bridges using the improved GLCME. This index enables efficient damage detection, with no spurious peaks observed at undamaged positions or curvature mode zero points, while distinct peaks emerge at target damage locations such as the mid-span, curvature mode zero points, and support-adjacent regions.

Both the curvature mode and the generalized local curvature mode information entropy inevitably produce peaks at the intermediate pier supports of continuous beams, and the peak values of the proposed index at the supports are significantly higher than those at the damage locations. However, the entropy values of all support peaks remain consistent. As marked in Fig. 8, the entropy value of the support peaks is approximately 0.348, and this value causes minimal interference with subsequent damage quantification based on NNs.

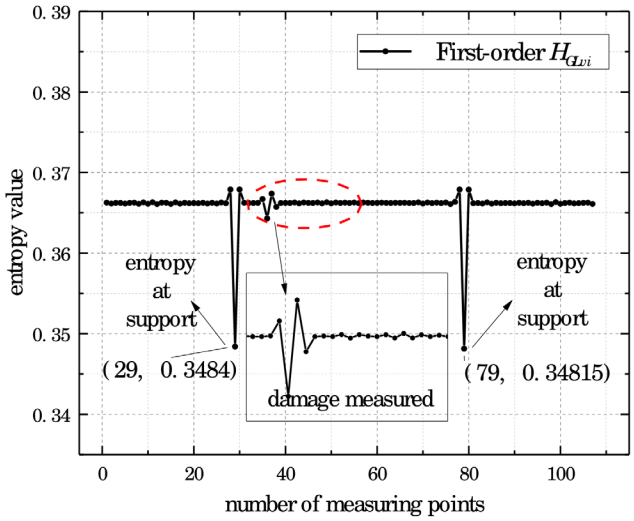
Across all test scenarios, the improved first-order index exhibits significantly superior damage identification performance at the mode shape nodes of the continuous beam (i.e., both ends of the middle span) compared to the mid-span region. This further verifies the high sensitivity of the index to damage near mode shape nodes.5.3 Construction and quantification results of the damage quantification NN.

To realize quantitative damage identification, training datasets were established for each damage location. The datasets included samples of the two indexes (curvature mode and generalized local curvature mode information entropy) under damage degrees of 10%, 15%, 25%, and 30% at different locations (detailed data omitted). A three-layer NN was adopted for damage degree prediction.

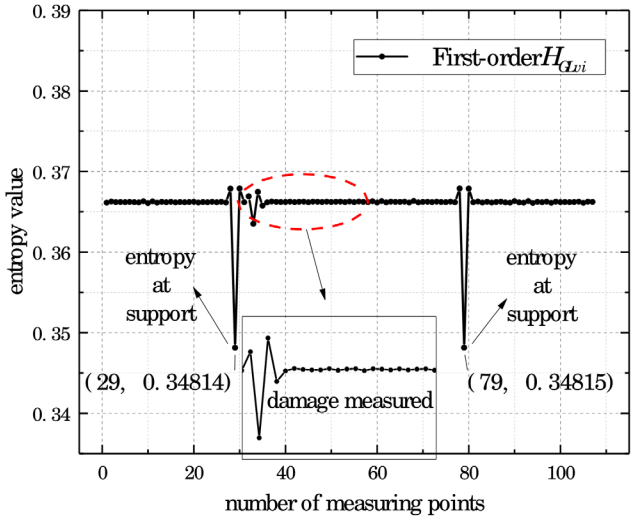
Based on the damage localization results in Section 5.2, the input parameters of the NN were defined as the index values (curvature mode and generalized local curvature mode information entropy) of three measurement points adjacent to the damage location. The optimal number of hidden layer nodes was determined as 5 via the bisection method. The output parameter was the residual stiffness of the damaged element. The network training parameters were set as follows: iteration steps = 50, training accuracy = 10^{-7}. A total of six NNs were constructed, corresponding to the



(a)



(b)



(c)

Fig. 13 Damage localization results of the continuous beam bridge: (a) Damage scenario 5-1; (b) Damage scenario 5-2; (c) Damage scenario 5-3

two indexes under three damage scenarios. The quantitative damage identification results are presented in Table 7.

Analysis of the results in Table 7 reveals the following insights:

The identification accuracy of the GLCME gradually improves as the damage location approaches the ends of the mid-span. For scenario 5-1 (mid-span damage), the relative error of the proposed index is 11.03%; while for scenario 5-3 (damage near the mode shape node), the relative error is reduced to only 1.43%. This confirms the high sensitivity of the index to damage adjacent to mode shape nodes.

Compared with the curvature mode, the proposed index exhibits lower quantitative accuracy for mid-span damage in continuous beams (scenario 5-1). However, in scenarios 5-2 and 5-3 (damage near curvature mode zero points and mode shape nodes), the relative error of the proposed index is significantly smaller than that of the curvature mode. This demonstrates that the proposed index outperforms the curvature mode in identifying damage near mode shape nodes for both continuous and simply supported beams, verifying the complementary nature of the two indexes.

It is noteworthy that the curvature mode also achieves satisfactory accuracy for damage far from mode shape nodes. Therefore, in practical engineering applications, if the potential damage location is preliminarily known, selecting appropriate identification indexes based on the specific location can effectively improve the efficiency and accuracy of damage assessment.

When considering damage near intermediate supports of continuous beams, the inherent entropy peaks from support constraints do not mask damage signals, as GLCME can distinguish them by their amplitude stability: support-induced peaks remain constant, while damage-induced peaks increase with severity. A minor limitation is that partial peak overlap may occur for damage immediately adjacent to supports, which can be mitigated by optimizing the sliding window size.

6 Conclusions

This study proposes a generalized local curvature mode information entropy index for structural damage identification and systematically verifies its performance through numerical simulations and physical experiments on simply supported beams, followed by an extension to continuous beam bridges. The key conclusions are summarized as follows:

1. In the numerical simulation of simply supported beams, the proposed generalized local curvature mode information entropy achieves accurate damage localization.

Table 7 Quantitative identification results of continuous beam bridge damage

Damage Scenario	CM	GLCME	Ideal output	Absolute error of CM	Absolute error of GLCME	Relative error of CM	Relative error of GLCME
5-1	0.877	0.888	0.8	7.70%	8.83%	9.62%	11.03%
5-2	0.705	0.849	0.8	9.54%	4.88%	11.93%	6.10%
5-3	0.820	0.811	0.8	2.02%	1.14%	2.53%	1.43%

When combined with a NN for damage quantification, the first two orders of the proposed index exhibit higher accuracy than the traditional curvature mode in identifying damage near various mode shape nodes. In contrast, the curvature mode performs better for damage far from mode shape nodes, indicating the complementary advantages of the two indexes.

2. Physical experiments on simply supported steel beams further validate the feasibility and superiority of the proposed index. The index effectively avoids the "node effect" that plagues the curvature mode, reducing the relative error of damage quantification near mode shape nodes from 72.9% to 20.0%, thereby significantly improving identification reliability.
3. For continuous beam bridges, the proposed index consistently exhibits characteristic peaks at supports with stable entropy values, which minimally interferes with damage identification. Despite the complex mechanical behavior of continuous beams (e.g., negative bending moments and curvature mode zero points), the index still achieves accurate damage localization and quantification, maintaining the same performance characteristics as observed in simply supported beams.
4. The complementary application of the generalized local curvature mode information entropy and the traditional curvature mode provide a more comprehensive and reliable solution for structural damage assessment. In practical engineering, this hybrid approach can be tailored to different damage locations to maximize identification accuracy and efficiency.

Future research will focus on extending the GLCME index to complex structures such as cable-stayed bridges and incorporating environmental perturbations to enhance its practical engineering applicability. Temperature fluctuations and ambient vibrations will be key factors to consider in this process. Additionally, damage migration simulations will be conducted. Damage locations will be systematically shifted along structural members and corresponding GLCME responses will be mapped to further validate the method's robustness. Moreover, the applicability boundary of the method will be further expanded through the optimization of vibration mode interpolation algorithms to accommodate extremely sparse sensing conditions.

Acknowledgments

This work was supported by the National Natural Science Foundation of China [Grant number 51868045] and the Innovation and R&D Team for Intelligent O&M Technology and Advanced Equipment of Architecture and Transportation Infrastructure [Grant number 2024-KYYWF-1109].

References

[1] Liu, Q., Xu, B., Zhu, X., Chen, R., Ge, H. "Experimental Study on Interface Debonding Defect Detection and Localization in Underwater Grouting Jacket Connections with Surface Wave Measurements", Sensors, 25(11), 3277, 2025. https://doi.org/10.3390/s25113277

[2] Zhou, L., Yan, G., Wang, L., Ou, J. "Review of Benchmark Studies and Guidelines for Structural Health Monitoring", Advances in Structural Engineering, 16(7), pp. 1187–1206, 2013. https://doi.org/10.1260/1369-4332.16.7.1187

[3] Han, D., Hosamo, H., Ying, C., Nie, R. "A Comprehensive Review and Analysis of Nanosensors for Structural Health Monitoring in Bridge Maintenance: Innovations, Challenges, and Future Perspectives", Applied Sciences, 13(20), 11149, 2023. https://doi.org/10.3390/app132011149

[4] Park, J. S., An, J., Park, H. S. "Computer Vision-based Structural Health Monitoring: A Review", International Journal of High-Rise Buildings, 12(4), pp. 321–333, 2023. https://doi.org/10.21022/IJHRB.2023.12.4.321

[5] Zhang, L., Liu, J., Sun, X., Jiang, X., Zou, Z., Li, X. "A review of bridge structural health monitoring based on different optical acquisition modules", Measurement, 257, 118922, 2025. https://doi.org/10.1016/j.measurement.2025.118922

[6] Civera, M., Surace, C. "Non-Destructive Techniques for the Condition and Structural Health Monitoring of Wind Turbines: A Literature Review of the Last 20 years", Sensors, 22(4), 1627, 2022. https://doi.org/10.3390/s22041627

[7] Ručevskis, S., Wesolowski, M. "Identification of Damage in a Beam Structure by Using Mode Shape Curvature Squares", Shock and Vibration, 17(4–5), 729627, 2010.
https://doi.org/10.3233/SAV-2010-0551

[8] Dongming, F., Feng, M. Q. "Output-only damage detection using vehicle-induced displacement response and mode shape curvature index", Structural Control and Health Monitoring, 23(8), pp. 1088–1107, 2016.
https://doi.org/10.1002/stc.1829

[9] Yan, G., Peng, X., Hao, H. "Localization of free-spanning damage using mode shape curvature", Journal of Physics: Conference Series, 305(1), 012017, 2011.
https://doi.org/10.1088/1742-6596/305/1/012017

[10] Zhong, H., Yang, M. "Damage detection for plate-like structures using generalized curvature mode shape method", Journal of Civil Structural Health Monitoring, 6(1), pp. 141–152, 2016.
https://doi.org/10.1007/s13349-015-0148-1

[11] Chen, Z., Zhang, R., Zheng, J.,Sun, H. "Sparse Bayesian learning for structural damage identification", Mechanical Systems and Signal Processing, 140, 106689, 2020.
https://doi.org/10.1016/j.ymssp.2020.106689

[12] Modesti, M., Reynders, E., Lombaert, G., Palermo, A., Gentilini, C. "Damage Detection in Beam Structures Based on Curvature Change Estimated from Incomplete Mode Shapes", Journal of Physics: Conference Series, 2647(18), 182019, 2024.
https://doi.org/10.1088/1742-6596/2647/18/182019

[13] Chandrashekhar, M., Ganguli, R. "Structural Damage Detection Using Modal Curvature and Fuzzy Logic", Structural Health Monitoring: An International Journal, 8(4), pp. 267–282, 2009.
https://doi.org/10.1177/1475921708102088

[14] Huang, T., Schröder, K. U. "A Bayesian probabilistic approach for damage identification in plate structures using responses at vibration nodes", Mechanical Systems and Signal Processing, 146, 106998, 2021.
https://doi.org/10.1016/j.ymssp.2020.106998

[15] Cao, M., Xu, W., Ostachowicz, W., Su, Z. "Damage identification for beams in noisy conditions based on Teager energy operator–wavelet transform modal curvature", Journal of Sound and Vibration, 333(6), pp. 1543–1553, 2014.
https://doi.org/10.1016/j.jsv.2013.11.003

[16] Ren, X., Meng, Z. "Damage identification for timber structure using curvature mode and wavelet transform", Structures, 60, 105798, 2024.
https://doi.org/10.1016/j.istruc.2023.105798

[17] Brownjohn, J. M. W. "Structural health monitoring of civil infrastructure", Philosophical Transactions of the Royal Society A: Mathematical, Physical and Engineering Sciences, 365(1851), pp. 589–622, 2006.
https://doi.org/10.1098/rsta.2006.1925

[18] Sharma, V. B., Singh, K., Gupta, R., Joshi, A., Dubey, R., …, Biswas, S. "Review of Structural Health Monitoring Techniques in Pipeline and Wind Turbine Industries", Applied System Innovation, 4(3), 59, 2021.
https://doi.org/10.3390/asi4030059

[19] Cosoli, G., Martarelli, M., Mobili, A., Tittarelli, F., Revel, G. M. "Damage Identification in Cement-Based Structures: A Method Based on Modal Curvatures and Continuous Wavelet Transform", Sensors, 23(22), 9292, 2023.
https://doi.org/10.3390/s23229292

[20] Anwar, A. M., Abd Elwaly, A. M. A. "Modal displacement vs Curvature functions as damage identifier for masonry structures", Alexandria Engineering Journal, 68, pp. 527–538, 2023.
https://doi.org/10.1016/j.aej.2023.01.042

[21] Shannon, C. E. "A mathematical theory of communication", The Bell System Technical Journal, 27(3), pp. 379–423, 1948.
https://doi.org/10.1002/j.1538-7305.1948.tb01338.x

[22] Lin, J. "Divergence measures based on the Shannon entropy", IEEE Transactions on Information Theory, 37(1), pp. 145–151, 1991.
https://doi.org/10.1109/18.61115

[23] Bandt, C., Pompe, B. "Permutation Entropy: A Natural Complexity Measure for Time Series", Physical Review Letters, 88(17), 174102, 2002.
https://doi.org/10.1103/PhysRevLett.88.174102

[24] Ren, W. X., Sun, Z. S. "Structural damage identification by using wavelet entropy", Engineering Structures, 30(10), pp. 2840–2849, 2008.
https://doi.org/10.1016/j.engstruct.2008.03.013

[25] Guan, X., Giffin, A., Jha, R., Liu, Y. "Maximum relative entropy-based probabilistic inference in fatigue crack damage prognostics", Probabilistic Engineering Mechanics, 29, pp. 157–166, 2012.
https://doi.org/10.1016/j.probengmech.2011.11.006

[26] Yang, Z., Chen, X., Jiang, Y., He, Z. "Generalised local entropy analysis for crack detection in beam-like structures", Nondestructive Testing and Evaluation, 29(2), pp. 133–153, 2014.
https://doi.org/10.1080/10589759.2014.904312

[27] Xiang, C. S., Li, L. Y., Zhou, Y., Yuan, Z. "Damage Identification Method of Beam Structure Based on Modal Curvature Utility Information Entropy", Advances in Civil Engineering, 2020(1), 8892686, 2020.
https://doi.org/10.1155/2020/8892686

[28] Alamdari, M. M., Samali, B., Li, J., Lu, Y., Mustapha, S. "Structural condition assessment using entropy-based time series analysis", Journal of Intelligent Material Systems and Structures, 28(14), pp. 1941–1956, 2017.
https://doi.org/10.1177/1045389X16679288

[29] Li, H., Bao, Y., Ou, J. "Structural damage identification based on integration of information fusion and Shannon entropy", Mechanical Systems and Signal Processing, 22(6), pp. 1427–1440, 2008.
https://doi.org/10.1016/j.ymssp.2007.11.025

[30] Limongelli, M. P., Giordano, P. F. "Vibration-based damage indicators: a comparison based on information entropy", Journal of Civil Structural Health Monitoring, 10(2), pp.251–266, 2020.
https://doi.org/10.1007/s13349-020-00381-9

[31] Yang, X., del Rey Castillo, E., Zou, Y., Wotherspoon, L. "UAV-deployed deep learning network for real-time multi-class damage detection using model quantization techniques", Automation in Construction, 159, 105254, 2024.
https://doi.org/10.1016/j.autcon.2023.105254

[32] Vivek, D., Supriya, G., Chaitanya, G. S., Dash, P. "A Deep Learning Approach for Real Time Road Damage Detection via Image Processing", International Journal of Scientific Research in Engineering and Management, 8(12), pp. 1–6, 2024. https://doi.org/10.55041/IJSREM39536

[33] Ge, Q., Li, C., Yang, F. "Research on the Application of Deep Learning Algorithm in the Damage Detection of Steel Structures", IEEE Access, 13, pp. 76732–76746, 2025. https://doi.org/10.1109/ACCESS.2025.3560640

[34] Mythili, M., Janani, D., Madhumitha, D. S., Mangala Madhumita, V..,Nandhini, R. "A Framework For Precise Road Damage Detection Using Deep Learning", In: 2024 2nd International Conference on Artificial Intelligence and Machine Learning Applications (AIMLA), Namakkal, India, 2024, pp. 1–5. ISBN 979-8-3503-4923-8 https://doi.org/10.1109/AIMLA59606.2024.10531516

[35] Abdullah, M., Pan, D. "Vibration-based structural damage detection for glass curtain walls using deep-learning algorithm", Signal, Image and Video Processing, 19(10), 788, 2025. https://doi.org/10.1007/s11760-025-04354-7

[36] Huang, L., Fan, G., Li, J., Hao, H. "Deep learning for automated multiclass surface damage detection in bridge inspections", Automation in Construction, 166, 105601, 2024. https://doi.org/10.1016/j.autcon.2024.105601

[37] Yamaguchi, T., Mizutani, T. "A Physics-Informed Neural Network for the Nonlinear Damage Identification in a Reinforced Concrete Bridge Pier Using Seismic Responses", Structural Control and Health Monitoring, 2024(1), 5532909, 2024. https://doi.org/10.1155/2024/5532909

[38] Cha, Y. J., Choi, W., Büyüköztürk, O. "Deep Learning-Based Crack Damage Detection Using Convolutional Neural Networks", Computer-Aided Civil and Infrastructure Engineering, 32(5), pp. 361–378, 2017. https://doi.org/10.1111/mice.12263

[39] Cha, Y. J., Choi, W., Suh, G., Mahmoudkhani, S., Büyüköztürk, O. "Autonomous Structural Visual Inspection Using Region-Based Deep Learning for Detecting Multiple Damage Types", Computer-Aided Civil and Infrastructure Engineering, 33(9), pp. 731–747, 2018. https://doi.org/10.1111/mice.12334

[40] Ding, H., Zhang, R., Zhang, Y., Xia, W., Huang, J. "A Bridge in China Externally Prestressed by Carbon Fiber-Reinforced Polymer Tendons", Structural Engineering International, 21(3), pp. 346–348, 2011. https://doi.org/10.2749/101686611X13049248220168

[41] MIDAS Information Technology Co. Ltd. "MIDAS/Civil, (Version 2018)", [computer program] Available at: https://www.midasit.com/ [Accessed: 15 April 2024]

[42] ANSYS Inc. "ANSYS Mechanical APDL, (Version 18.0)", [computer program] Available at: https://www.ansys.com/ [Accessed: 15 April 2024]